Nanoscale characterization of individual horizontally aligned single-walled carbon nanotubes

Gergely Németh[*,1], Áron Pekker[1], Dániel Datz[1], Hajnalka Mária Tóháti[1], Keigo Otsuka[2], Taiki Inoue[2], Shigeo Maruyama[2], Katalin Kamarás[1]

[1] Institute for Solid State Physics and Optics, Wigner Research Centre for Physics, Hungarian Academy of Sciences, Budapest, Hungary
[2] Department of Mechanical Engineering, School of Engineering, The University of Tokyo, Tokyo, Japan

Received XXXX, revised XXXX, accepted XXXX
Published online XXXX

Key words: SNOM,nanotube,carbon,individual,aligned,horizontally,nanoscale,nano

[*] Corresponding author: e-mail nemeth.gergely@wigner.mta.hu, Phone: +36-30-6278845

One of the most challenging tasks in nanotube research is to identify the different electronic type of nanotubes for device fabrication. The implementation of standard spectroscopy techniques at the single-tube level has remained a great task due to small nanotube signal and low spatial resolution. Scattering-type scanning near-field optical microscopy (s-SNOM) yields information on the optical characteristics of the sample with high spatial resolution. We have already demonstrated that this method is able to distinguish between different electronic types of carbon nanotube bundles based on their optical properties in the infrared region. Now we applied the same method to characterize individual horizontally aligned single-walled carbon nanotubes (SWCNT).

1 Introduction Single-walled carbon nanotubes are still in the focus of research due to their unique physical properties. They are identified by their chirality which dictates the physical structure and electronic properties of the individual species. The selective production of carbon nanotubes is still under intense research for device fabrication like FET arrays [1], high performance electronics [2] and low noise amplifiers [3]. The characterization of the individual products of selective growth is an important and difficult task. Because of the size of individual nanotubes, it is still a challenge. The diffraction-limited spatial resolution of standard optical methods being insufficient for the study of objects of such size, alternative methods have to be used. Scattering-type scanning near-field optical microscopy combines high spatial resolution with low detection threshold of optical properties of materials even on the nanoscale.

2 Experimantal methods The scattering-type near-field optical microscope setup provides completely wavelength-independent resolution. It is basically the combination of an atomic force microscope (AFM) and a Michelson interferometer (Fig. 1). The AFM part employs standard Si probing tips with metal coating. The end of the tip is illuminated with a focused laser beam. The light from this laser induces a strong evanescent electromagnetic field which can interact with the sample. The interaction between the near-field and the sample influences the back-scattered light in a way that can be described by a complex scattering coefficient ($\sigma = se^{i\varphi}$). The light scattered back along the illumination path is collected and recorded as the optical signal.

Because only a small part of the scattered light is coming from the tip, the AFM is working in tapping mode to modulate the near-field interaction and the scattered light is analyzed by pseudo-heterodyne detection with the interferometer. Demodulating the acquired signal at higher harmonics (nth) of the tip oscillation frequency (Ω), we can obtain the amplitude (s_n) and the phase (φ_n) of the scattered light [4]. The higher order we demodulate the sig-

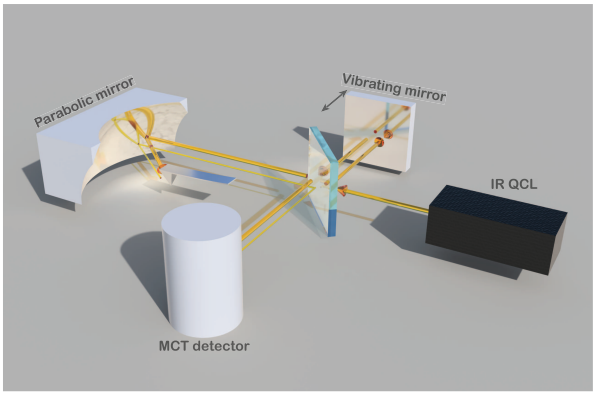

Figure 1 Schematic illustration of the s-SNOM device. The source of the incoming light is an infrared quantum cascade laser (IR QCL) and for the detection we used an MCT detector.

nal the more it will contain from the near-field scattering. In our experiments we used the second (O2) and the third (O3) harmonic demodulation.

Our s-SNOM instrument was produced by Neaspec GmbH. As probing tip we used commercially available Pt-coated Si AFM tips purchased from NanoWorld. The illuminating unit was a tunable quantum cascade laser (QCL) with frequency range $960 - 1020\,\mathrm{cm}^{-1}$.

3 Sample preparation The horizontally aligned SWCNTs were individually grown by CVD technique. After the growing phase the nanotubes were transferred between gold contacts generated by lithography on a Si/SiO_2 substrate [5]. Metallic nanotubes were subsequently destroyed by the electrical breakdown technique [5–7]. Scanning electron microscopy (SEM) images of the samples before and after breaking the metallic nanotubes are shown in Fig. 2.

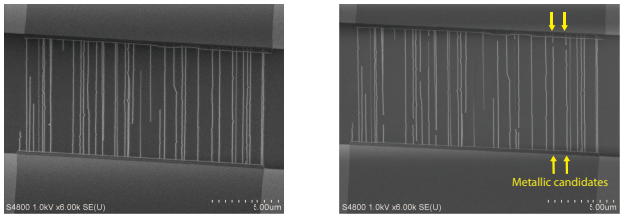

Figure 2 SEM images of the horizontally aligned SWCNT sample, before (left) and after (right) breaking metallic SWCNTs. Two metallic candidates are marked in the area of interest.

4 Optical properties of CNT bundles We performed our s-SNOM measurements in the infrared region between 960-1020 cm^{-1} with our QCL laser. In this spectral region the optical properties originate from the excitation of the free charge carriers. The difference between the free carrier density of the semiconducting and metallic nanotubes leads to a difference in the dielectric permittivity. A broad peak in the dielectric function belongs to the zero frequency Drude peak. Fig. 3 presents the complex dielectric permittivity $(\epsilon = \epsilon_1 + i\epsilon_2)$ of separated semiconducting and metallic nanotubes. The spectra were acquired from transmittance measurements performed on nanotube thin films and calculated via Kramers-Kronig analysis [8].

Because of the different absorption of the two types of nanotubes we expect distinct near-field phase contrast between the substrate and the two kinds of nanotube. We note that in s-SNOM measurements we always normalize all data to the signal of the substrate.

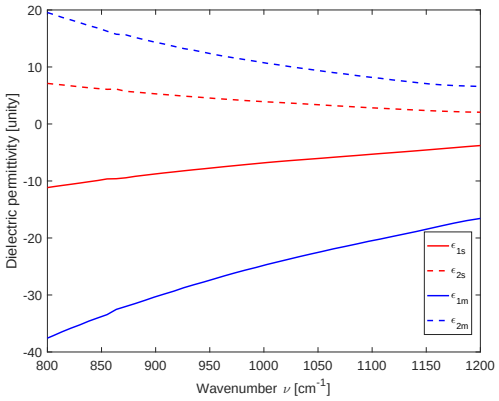

Figure 3 The real (solid) and imaginary part (dashed) of the dielectric function in case of metallic (blue) and semiconducting (red) nanotube samples.

In our previous study we predicted the difference in the near-field scattered signal in case of metallic or semiconducting nanotube bundles by using the Extended Finite Dipole Model (EFDM) [9]. This model approximates the tip-nanosphere-substrate system with several dipoles. We exchanged the nanosphere to a cylinder by replacing its polarizability to that of a prolate ellipsoid with high aspect ratio [10].

The outcome of this calculation [11] is shown in Fig.4. The results verify our expectations. The calculation yields that the metallic nanotubes have higher near-field phase signal relative to the substrate. The near-field phase contrast of the semiconducting nanotubes remains near zero in the range of interest.

5 Results and discussion We performed the s-SNOM experiment on the sample mentioned above. The nanotubes are located between the gold contacts, on a SiO_2 substrate. The optical properties of the substrate are crucial for the measurement, as the substrate has to provide appreciable near-field signal in order to have the appropriate coupling between the nanoparticle and the tip. Fortunately

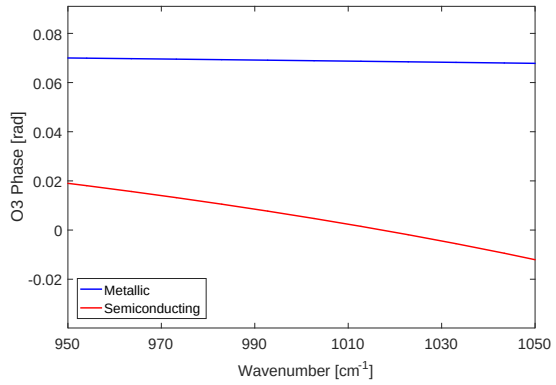

Figure 4 The result of the EFDM calculation for third harmonic demodulated (O3) near-field phase signal for metallic (blue) and semiconducting (red) nanotube bundles with diameter of $4\,\mathrm{nm}$. All data were normalized to the substrate.

SiO_2 has almost as high near-field scattering as Si in this infrared region.

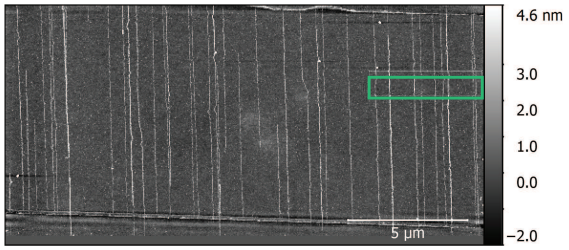

Figure 5 AFM topography image of the horizontally aligned nanotube sample. The green box represents the region of interest for the high resolution measurements which has two metallic nanotubes candidates amongst several semiconducting nanotubes.

The AFM topography map of the sample can be seen in Fig.5. For high resolution s-SNOM measurements we chose a clean area (indicated by the green rectangle) where the nanotubes are properly separated to measure them individually. The chosen area contains two metallic nanotube candidates.

The outcome of the high resolution third-harmonic demodulated measurements at $985\,\mathrm{cm}^{-1}$ is presented in Fig.6. The upper map is the corresponding AFM topography. The blue boxes indicate the metallic nanotube candidates. The diameter of these metallic tubes are approximately $3\,\mathrm{nm}$ and $1.7\,\mathrm{nm}$. The third-harmonic demodulated phase map (φ_{O3}) was acquired simultaneously and is presented in the lower part of Fig.6. The phase responses of the individual nanotubes are similar to those of the bundles. We find that the two metallic candidates give the highest phase response, with the larger tube showing $\varphi_{O3} \approx 0.168\,[\mathrm{rad}]$ and the smaller $\varphi_{O3} \approx 0.132\,[\mathrm{rad}]$. It is very important to note that in general the size of the nanoparticle influences the near-field contrast between the substrate and the particle [12].

The O3 phase map also shows that the largest semiconducting tube $(2.5\,\mathrm{nm})$ (red box) exhibits a lower phase signal than the smallest metallic one. Based on these observations we can declare that all nanotubes in this area with lower phase contrast than the $1.7\,\mathrm{nm}$ metallic carbon nanotube, are semiconducting ones.

We also examined the spectral behavior of these individual nanotubes. Fig. 7 shows the result of these measurements. We can conclude from the spectra that the frequency dependence of the near-field phase signal follows that of the imaginary part of the dielectric function.

We find that at higher wavenumbers $(1025\,\mathrm{cm}^{-1})$ the phase of the semiconducting nanotubes is obstructed by the noise, but the phase of the metallic ones is still detectable.

6 Conclusions In our study we found that near-field infrared imaging of individual SWCNTs is possible even on a SiO_2 substrate. We proved that the electrical breakdown technique destroys partially only the metallic nanotubes. The spectroscopic study verifies that the near-field phase is connected with the imaginary part of the dielectric function.

Acknowledgements Research supported by the Hungarian National Research Fund (OTKA) No. SNN 118012.

References

[1] S. J. Kang, C. Kocabas, T. Ozel, M. Shim, N. Pimparka, M. A. Alam, S. V. Rotkin, and J. A. Rogers, Nature Nanotechnology **2**, 230–236 (2007).
[2] D. Sun, M. Y. Timmermans, Y. Tian, A. G. Nasibulin, E. I. Kauppinen, S. Kishimoto, T. Mizutani, and Y. Ohno, Nature Nanotechnology **6**, 156–161 (2011).
[3] K. Parrish, Carbon nanotube transistors for a low noise amplifier: Feasibility and future (2010).
[4] R. Hillenbrand and F. Keilmann, Appl. Phys. Lett. **89**(101124), 1–3 (2006).
[5] P. G. Collins, M. S. Arnold, and P. Avouris, Science **292**, 706–709 (2001).
[6] K. Otsuka, T. Inoue, S. Chiashi, and S. Maruyama, Nanoscale **6**, 8831–8835 (2014).
[7] K. Otsuka, T. Inoue, Y. Shimomura, S. Chiashi, and S. Maruyama, Nanoscale **8**, 16363–16370 (2016).
[8] H. M. Tóháti, Á. Pekker, B. Á. Pataki, Z. Szekrényes, and K. Kamarás, Eur. Phy. J. B **87**, 126 (2014).
[9] N. Ocelic, Quantitative Near-field Phonon-polariton Spectroscopy, PhD thesis, Technical University Munich, 2007.
[10] J. Venermo and A. Sihvola, Journal of Electrostatics **63**, 101–117 (2005).
[11] G. Németh, D. Datz, H. M. Tóháti, Á. Pekker, and K. Kamarás, physica status solidi (b) **253**, 2413–2416 (2016).
[12] A. Cvitkovic, Substrate-Enhanced Scattering-Type Scanning Near-Field Infrared Microscopy of Nanoparticles, PhD thesis, Technische Universität München, 2009.

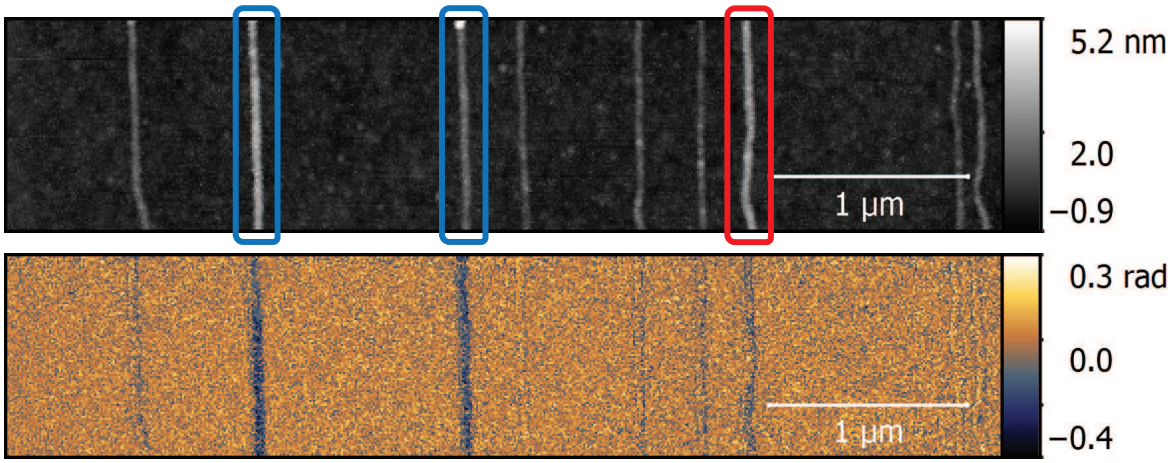

Figure 6 AFM topography image of the chosen area for high resolution s-SNOM measurements (above) and the O3 near-field phase map at $985\,\mathrm{cm}^{-1}$ of the same area (below). The blue boxes indicate the metallic nanotube candidates. The red box stands for the largest semiconducting nanotube.

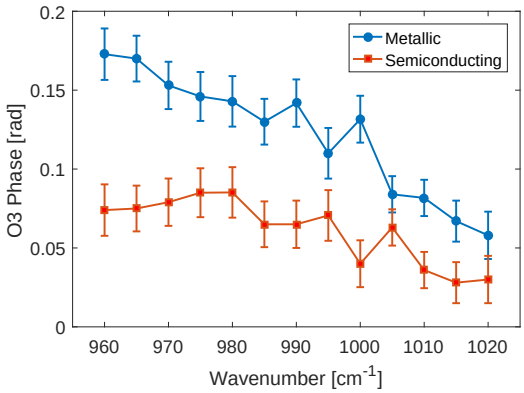

Figure 7 Third-harmonic demodulated (O3) near-field phase spectra of a semiconducting (red) and metallic (blue) carbon nanotube.